



**HAL**  
open science

## Loss of lung microvascular endothelial Piezo2 expression impairs NO synthesis, induces EndMT, and is associated with pulmonary hypertension

Siyu Tian, Zongye Cai, Payel Sen, Denise van Uden, Esther van de Kamp, Raphael Thuillet, Ly Tu, Christophe Guignabert, Karin Boomars, Kim van der Heiden, et al.

### ► To cite this version:

Siyu Tian, Zongye Cai, Payel Sen, Denise van Uden, Esther van de Kamp, et al.. Loss of lung microvascular endothelial Piezo2 expression impairs NO synthesis, induces EndMT, and is associated with pulmonary hypertension. *AJP - Heart and Circulatory Physiology*, 2022, 323 (5), pp.H958 - H974. 10.1152/ajpheart.00220.2022 . inserm-04270340

**HAL Id: inserm-04270340**

**<https://inserm.hal.science/inserm-04270340>**

Submitted on 4 Nov 2023

**HAL** is a multi-disciplinary open access archive for the deposit and dissemination of scientific research documents, whether they are published or not. The documents may come from teaching and research institutions in France or abroad, or from public or private research centers.

L'archive ouverte pluridisciplinaire **HAL**, est destinée au dépôt et à la diffusion de documents scientifiques de niveau recherche, publiés ou non, émanant des établissements d'enseignement et de recherche français ou étrangers, des laboratoires publics ou privés.

# Loss of lung microvascular endothelial Piezo2 expression impairs NO synthesis, induces EndMT, and is associated with pulmonary hypertension

Siyu Tian,<sup>1</sup> Zongye Cai,<sup>1</sup> Payel Sen,<sup>2,3</sup> Denise van Uden,<sup>4</sup> Esther van de Kamp,<sup>1</sup> Raphael Thuillet,<sup>5,6</sup> Ly Tu,<sup>5,6</sup> Christophe Guignabert,<sup>5,6</sup> Karin Boomars,<sup>4</sup> Kim Van der Heiden,<sup>7</sup> Maarten M. Brandt,<sup>1</sup> and Daphne Merkus<sup>1,2,3</sup>

<sup>1</sup>Experimental Cardiology, Department of Cardiology, Thoraxcenter, Erasmus University Medical Center, Rotterdam, The Netherlands; <sup>2</sup>Walter Brendel Center of Experimental Medicine, University Clinic Munich, Munich, Germany; <sup>3</sup>German Center for Cardiovascular Research, Partner Site Munich, Munich Heart Alliance, Munich, Germany; <sup>4</sup>Department of Pulmonary Medicine, Erasmus MC, University Medical Center, Rotterdam, The Netherlands; <sup>5</sup>INSERM UMR\_S 999, Hôpital Marie Lannelongue, Le Plessis-Robinson, France; <sup>6</sup>School of Medicine, Université Paris-Saclay, Le Kremlin-Bicêtre, France; and <sup>7</sup>Biomedical Engineering, Department of Cardiology, Thoraxcenter, Erasmus University Medical Center, Rotterdam, The Netherlands

## Abstract

Mechanical forces are translated into biochemical stimuli by mechanotransduction channels, such as the mechanically activated cation channel Piezo2. Lung Piezo2 expression has recently been shown to be restricted to endothelial cells. Hence, we aimed to investigate the role of Piezo2 in regulation of pulmonary vascular function and structure, as well as its contribution to development of pulmonary arterial hypertension (PAH). The expression of Piezo2 was significantly reduced in pulmonary microvascular endothelial cells (MVECs) from patients with PAH, in lung tissue from mice with a *Bmpr2*<sup>+/<sup>R899X</sup></sup> knock-in mutation commonly found in patients with pulmonary hypertension, and in lung tissue of monocrotaline (MCT) and sugen-hypoxia-induced PH (SuHx) PAH rat models, as well as from a swine model with pulmonary vein banding. In MVECs, Piezo2 expression was reduced in response to abnormal shear stress, hypoxia, and TGF $\beta$  stimulation. Functional studies in MVECs exposed to shear stress illustrated that siRNA-mediated Piezo2 knockdown impaired endothelial alignment, calcium influx, phosphorylation of AKT, and nitric oxide production. In addition, siPiezo2 reduced the expression of the endothelial marker PECAM-1 and increased the expression of vascular smooth muscle markers ACTA2, SM22a, and calponin. Thus, Piezo2 acts as a mechanotransduction channel in pulmonary MVECs, stimulating shear-induced production of nitric oxide and is essentially involved in preventing endothelial to mesenchymal transition. Its blunted expression in pulmonary hypertension could impair the vasodilator capacity and stimulate vascular remodeling, indicating that Piezo2 might be an interesting therapeutic target to attenuate progression of the disease.

**NEW & NOTEWORTHY** The mechanosensory ion channel Piezo2 is exclusively expressed in lung microvascular endothelial cells (MVECs). Patient MVECs as well as animal models of pulmonary (arterial) hypertension showed lower expression of Piezo2 in the lung. Mechanistically, Piezo2 is required for calcium influx and NO production in response to shear stress, whereas stimuli known to induce endothelial to mesenchymal transition (EndMT) reduce Piezo2 expression in MVECs, and Piezo2 knockdown induces a gene and protein expression pattern consistent with EndMT.

*endothelial-to-mesenchymal transition; lung microvascular endothelial cell; Piezo2 channel; pulmonary hypertension; shear stress*

## INTRODUCTION

The pulmonary vasculature comprises a low-pressure, high-flow circulation, with a much lower resistance as compared with the systemic circulation. Oxygen concentrations in the lungs are normally high, and there is little metabolically active tissue, precluding metabolic vasodilation in regulation of

pulmonary vascular tone. As such, pulmonary vascular tone regulation is different from that in the systemic vasculature and is largely dependent on shear stress-dependent regulation of endothelial function (1). Hence, mechanosensing and mechanotransduction are important processes in regulation of pulmonary vasomotor tone and pulmonary vascular resistance (PVR). Depending on intensity and duration, alterations

Correspondence: D. Merkus (d.merkus@erasmusmc.nl).

Submitted 6 May 2022 / Revised 21 September 2022 / Accepted 21 September 2022

*Am J Physiol Heart Circ Physiol* 323: H958–H974, 2022.

in mechanical forces may not only have acute effects, modulating the release of vasoactive components, such as nitric oxide (NO) and endothelin, but also cause long-term effects such as inflammation, contributing to endothelial to mesenchymal transition (EndMT) (2–5), and structural remodeling through obstruction of the distal pulmonary arterioles (6). Thus, altered mechanical forces are increasingly recognized to contribute to the development of pulmonary vascular disease in general and pulmonary arterial hypertension (PAH) in particular (7). PAH is characterized by an imbalance in TGF $\beta$ -bone morphogenetic protein (BMP) signaling, leading to endothelial dysfunction and hyperproliferation, as well as muscularization of the distal pulmonary vasculature.

Mechanical forces are translated into biochemical stimuli by mechanotransduction channels, such as the mechanically activated Piezo (Piezo1 and Piezo2) cation channels (8). Piezo1 is vital for early vascular development and is involved in flow-mediated calcium influx in endothelial cells (9, 10). Piezo1 activation in response to changes in flow results in activation of inflammatory signaling and altered NO production in both systemic (11, 12) and pulmonary endothelial cells (13). Intriguingly, lung Piezo2 expression has been recently shown to be restricted to pulmonary endothelial cells (14). In metastatic cancer cells, Piezo2 modulates RhoA activity, formation of actin-based stress fibers, and orientation of focal adhesions (15), processes that also play a role in endothelial responses to shear stress. Whether Piezo2 plays a role in physiological regulation of PVR and/or whether its altered expression may contribute to development or progression of pulmonary vascular disease is currently unknown.

Here, we hypothesized that mechanosensing through Piezo2 plays a role in the regulation of pulmonary vascular function and that loss of Piezo2 may play a role in the development of pulmonary vascular disease. Consequently, our study aimed to elucidate 1) if expression of Piezo2 is altered in lung microvascular endothelial cells (MVECs) of patients with PAH, as well as in four animal models reflecting different stages and/or aspects of pulmonary hypertension (PH), *Bmpr2*<sup>+/*R899X*</sup> mice in which PH is caused by alterations in BMP signaling, and MCT and SuHx PAH rat models and swine with pulmonary vein banding (PVB), in which development of PH is accompanied by alterations in shear stress through redistribution of flow from the caudal (banded) lobes toward the unbanded cranial lobes; and 2) whether such altered Piezo2 expression may predispose to development of pulmonary vascular disease by altering pulmonary endothelial mechanosensing and subsequent acute (NO production) and long-term (endothelial alignment to flow, EndMT) cellular responses.

## MATERIAL AND METHODS

All animal experiments were performed in accordance with Directive No. 2010/63EU of the European parliament on the protection of animals used for scientific purposes, with the Guide for the Care and Use of Laboratory Animals, adopted by the National Institute of Health and with the approval of the Central Committee for Animal Experiments in The Netherlands [AVD101002016636 (swine), AVD1010020197725 (mice)], as well as the animal welfare body of the Erasmus University Medical Center.

Rat experiments were approved by the Ethics Committee of the Université Paris-Saclay (No. 11484).

### Mouse Model

*Bmpr2*<sup>+/*R899X*</sup> mice ( $n = 6$ ), which have a premature stop codon in the *Bmpr2* gene leading to reduced BMPRII expression, have been previously described (16). *Bmpr2*<sup>+/*+*</sup> littermates served as wild-type (WT) controls ( $n = 7$ ). Mice were bred and housed at the Erasmus University Medical Center under specific pathogen-free (SPF) conditions, fed ad libitum, and had free access to drinking water. Mice were euthanized and analyzed when 31 wk old as previously described (17). In short, mice were anesthetized by an intraperitoneal injection with urethane (2 mg/g). Urethane was used since this anesthetic has a minimal effect on the cardiovascular and respiratory system. An ultrasound measurement was performed to assess cardiac output. Subsequently, a tracheal canula (miniVent type 845, Hugo Sachs Elektronik, March-Hugstetten, Germany) was placed, the thorax was opened and the right ventricle (RV), and pressure was measured using a pressure catheter (Miller, Inc., Houston, TX) via apical puncture, after which heart and lungs were excised. RV and left ventricle (LV) + septum (S) were next separated and weighted separately. The Fulton index was calculated by dividing the weight of the RV by the weight of LV + S. The postcaval lung lobe was stored at  $-80^{\circ}\text{C}$  until processing of the material for gene expression.

### Rat Models

Two well-established rat models of severe PAH were used for this study (18, 19). Briefly, monocrotaline (MCT)-induced PH (MCT) was established in 4-wk-old male Wistar rats (Janvier Labs, Saint Berthevin, France), with a single subcutaneous injection of MCT (40 mg/kg, Sigma-Aldrich, Saint-Quentin-Fallavier, France), and evaluated after 3 wk (MCT-PH,  $n = 10$ ; and controls,  $n = 6$ ). Sugen-hypoxia-induced PH (SuHx) was established in 4-wk-old male Wistar rats (Janvier Labs, Saint Berthevin, France), by a single subcutaneous injection of SU5416 (20 mg/kg; Sigma-Aldrich, Saint-Quentin-Fallavier, France) combined with exposure to normobaric hypoxia for 3 wk followed by normoxia for 5 wk (SuHx-PH,  $n = 6$ ; and controls,  $n = 8$ ). After measurement of hemodynamic parameters, the thorax was opened and the left lung immediately removed and frozen until processing of gene expression experiments.

### Swine Model

Eighteen Yorkshire  $\times$  Landrace swine of either sex obtained from a commercial breeder (3 to 4 wk old,  $6 \pm 1$  kg) entered the study. Swine were individually housed in the animal center of the Erasmus University Medical Center, fed twice a day, and had free access to drinking water. Sedation was induced with an intramuscular injection of tiletamine-zolazepam (5 mg/kg; Virbac, Barneveld, The Netherlands), xylazine (2.25 mg/kg; AST Pharma, Oudewater, The Netherlands), and atropine (0.5 mg) for sedation and were subsequently anesthetized with an intravenous bolus of thiopental (10 mg/kg; Rotexmedica, Trittau, Germany). After relaxation of the vocal chords, an endotracheal tube was inserted and secured and ventilation was started [O<sub>2</sub>:N<sub>2</sub> (1:2)]. Anesthesia was maintained by adding

sevoflurane (2% vol/vol, Pharmachemie, Haarlem, The Netherlands) to the gas mixture. Pulmonary vein banding (PVB) of the confluent of the veins draining the caudal lung lobes was subsequently induced in 10 swine as previously described, resulting in progressive pulmonary hypertension (20, 21). Sham-operated animals served as control ( $n = 8$ ). All swine were chronically instrumented 4 wk after PVB, and hemodynamics, consisting of aortic blood pressure, pulmonary artery pressure (PAP), left atrial pressure, and cardiac output, were obtained with swine standing quietly 11 to 12 wk after PVB (20, 21). Twelve weeks after PVB, swine were anesthetized and euthanized by excision of the hearts and lungs. Lung tissue of the right caudal and cranial lobes was harvested for gene expression analysis and isolation of swine lung microvascular endothelial cells (sMVECs) as previously described (22). Briefly, lung tissue was submerged in collagenase type 2 (Worthington Biochemical Corp.) and incubated at 37°C for 20 min. The tissue was next placed in 10 mL of endothelial basal medium supplemented with 2 MV Bulletkit (Lonza, Basel, Switzerland) and 10 U/mL heparin (Leo Pharma, B.V., Amsterdam, The Netherlands), in which cells were squeezed out of the tissue via mechanical compression using a cell scraper. The resulting cell suspension was filtered with a 70- $\mu$ m filter (BD Bioscience, Breda, The Netherlands), after which the flow through was washed twice in culture medium and filtered once more using a 20- $\mu$ m filter (pluriSelect, Leipzig, Germany). Endothelial clusters cannot pass the 20- $\mu$ m filter and by flipping the filter upside down, these clusters could be eluted from the filter and seeded on fibronectin (Roche, Basel, Switzerland)-coated plates.

### Human Microvascular Endothelial Cells

Lung specimens were obtained after lung transplant of patients with idiopathic PAH (iPAH) and lobectomy or pneumonectomy for localized lung cancer of control subjects (see Table 1). Preoperative echocardiological evaluations, including echocardiography, were performed in the control subjects to rule out PAH, and the lung specimens from the control subjects were collected distant from the tumor foci.

**Table 1.** Baseline characteristics of all patients with PAH and non-PAH controls

	Patients with PAH	Controls
<i>n</i>	8	10
Age, yr	40 ± 13	76 ± 12
Sex, male/female	2/6	5/3
Mutation in BMPR2 gene, y/n	0/8	NA
NYHA functional class, I/II/III/IV	0/0/7/1	NA
6MWD, m	382 ± 110	NA
mPAP, mmHg	69 ± 26	NA
CI, L/min/m <sup>2</sup>	3.2 ± 0.6	NA
PVRi, mmHg/L/min/m <sup>2</sup>	9.2 ± 2.3	NA
PCWP, mmHg	11.4 ± 3.4	NA

Values are means ± SE; *n*, number of patients. NYHA, New York Heart Association; 6MWD, 6-min walking distance; mPAP, mean pulmonary artery pressure; CI, cardiac index; PVRi, pulmonary vascular resistance; PCWP, pulmonary capillary wedge pressure; PAH, pulmonary arterial hypertension; NA, not applicable.

**Table 2.** Donor characteristics of human MVECs used in *in vitro* experiments

	Assay	Sex	Age, yr
Controls			
Control 1	SS, PCR, IF, WB	F	68
Control 2	SS, PCR, IF, WB, ELISA	F	62
Control 3	SS, PCR, IF, WB, ELISA	M	40
PAH MVECs			
Patient 1	SS, PCR, IF	M	23
Patient 2	SS, PCR, IF	F	33

PAH, pulmonary arterial hypertension; MVEC, microvascular endothelial cell; SS, shear stress; PCR, polymerase chain reaction; IF, immunofluorescent staining; WB, Western blot; M, male; F, female.

### Isolation and Culture of Human Pulmonary ECs for Piezo Expression

Pulmonary MVECs were isolated and cultured as previously described (23). The isolated pulmonary MVECs were strongly positive for acetylated low-density lipoprotein (coupled to Alexa Fluor 488), vonWillebrand factor (vWF), CD31, and Ulex europaeus agglutinin-1 and negative for ACTA2.

### Human Primary Cell Culture

Human lung MVECs (Lonza) were obtained from three healthy donors. PAH lung microvascular endothelial cells (PAH-MVECs) were obtained from two iPAH donors. All cells were cultured in endothelial basal medium supplemented with 2 MV Bulletkit (Lonza) and 1× penicillin-streptomycin solution (Biowest, Alveringem, Belgium) in 5% CO<sub>2</sub> at 37°C. Confluent cells between *passage* 6–8 were used in the experiments. All results were obtained and confirmed in at least two donors. Donors' characteristics can be found in Table 2.

### Hypoxia and TGFβ2 Stimulation on Endothelial Cells

Human lung MVECs were seeded on 12-well plates and exposed to 1% O<sub>2</sub> for hypoxia (versus 21% O<sub>2</sub> for normoxic conditions) for 24 h. After 24-h hypoxia or normoxia, cells were lysed for RNA isolation. For TGFβ2 stimulation, MVECs were treated with 10 ng/mL of TGFβ2 (302-B2, R&D systems, Chatillon, France) for 96 h, after which cells were lysed for RNA isolation.

### Shear Stress Experiments

Human lung MVECs were seeded on  $\mu$ -Slide I 0.6 Luer Ibidi treated slides or  $\mu$ -Slide I 0.2 Luer Ibidi treated slides (Ibidi, Munich, Germany) depending on the shear stress values required. The number of cells seeded on the slides was according to the manufacturer's instructions. After seeding, cells were allowed to attach to the chambers for 24 h before initiating laminar flow. The chambers were connected with the red perfusion set and constant flow was applied by the Ibidi pump system (Ibidi, Munich, Germany). The flow system was maintained in 5% CO<sub>2</sub> at 37°C. Normal (21 dyn/cm<sup>2</sup>) and high shear stress (67 dyn/cm<sup>2</sup>) values were set according to values reported in small vessels in patients with pulmonary hypertension (52–116 dyn/cm<sup>2</sup>) and controls (20 dyn/cm<sup>2</sup>) (3, 7, 24). Shear stress was gradually increased over time for both normal shear stress (NSS, from 4 to 15 to 21 dyn/cm<sup>2</sup>

increase every 24 h) and high shear stress (HSS, from 8 to 21 to 67 dyn/cm<sup>2</sup> increase every 24 h). For studies on alignment to shear stress and Piezo gene expression, MVECs exposed to shear stress were compared with static controls on similar Ibidi slides.

### siRNA Transfection

Human lung MVECs at 70% confluence were transfected with 50 nmol nontargeting siRNA (D-001810-10-20, GE Healthcare Dharmacon, Cambridge, UK) and Piezo2 siRNA (J-013925-18-0002, GE Healthcare Dharmacon) using DharmaFECT 1 Transfection Reagent (T-2001-02, GE Healthcare Dharmacon). For improved efficiency, the siRNA transfection was repeated 24 h after the initial transfection, and cells were used for experiments 24 h after the second transfection.

### Live Cell Calcium Imaging

Human lung MVECs were seeded on the  $\mu$ -Slides I 0.4 Luer ibidi-treated slides and allowed to attach for 24 h. On the day of experiments, cells were loaded with 2  $\mu$ M Fluo-4AM ester (Thermo Fisher Scientific, Bleiswijk, The Netherlands) with 1 mM probenecid and 0.04% Pluronic F-127(AAT Bioquest). Slides were incubated for 30 min in 5% CO<sub>2</sub> at 37°C. Slides were then connected with the yellow/green perfusion (longer tubes, easy to fit in the confocal system) set to the Ibidi pump system. The Ibidi pump system and slides were then transferred to the stage of Leica SP5 confocal microscope of which the  $\times$ 20 objective and the 488-nm laser were used. Images were acquired at 1-s intervals for 5 min. The shear-induced excitation was normalized with the fluorescence intensity in the same slide under static condition. All imaging experiments were performed in 5% CO<sub>2</sub> at 37°C.

### Determination of Nitrite + Nitrate Levels

To determine flow-induced nitrite + nitrate release from endothelial cells,  $1 \times 10^5$  human lung MVECs cells were seeded on  $\mu$ -Slides I 0.4 Luer ibidi-treated slides. Twenty-four hours after seeding, cells were either kept under static conditions or exposed to normal shear stress. Forty-eight hours after onset of shear stress, culture medium was isolated from the ibidi  $\mu$ -Slides. Subsequently, this medium was used in the nitrite/nitrate fluorometric assay (780051, Cayman Chemical) according to the manufacturer's instructions. Nitrite + nitrate release was calculated by multiplying the concentration with the total medium volume.

### Quantitative Real-Time Polymerase Chain Reaction

RNA isolation was performed in different laboratories, using different protocols. Total RNA was isolated from lung tissue from PAH rat models, as well as from PAH and control MVECs using RNeasy mini kit (Qiagen, Valencia, CA). Total RNA (1  $\mu$ g) was reverse transcribed using High-Capacity RNA-to-cDNA kit (Invitrogen, Carlsbad, CA) according to manufacturer's instructions. RT-qPCR was performed on Step-One Plus Real-Time PCR machine (Applied Biosystems). Gene expression levels were quantified using preverified Assays TaqMan primer/probe sets: Taqman assays for Piezo1Hs00207230\_m1 and for Piezo2 Hs00926218\_m1 (Applied Biosystems, Foster

City, CA). The expression level of each gene was normalized to 18S ribosomal RNA (4319413E, Applied Biosystems) using the comparative  $\Delta\Delta$ Ct method.

For porcine lung tissue, as well as following the experiments in which human MVECs were exposed to different stimuli, total RNA was isolated using the ISOLATE II RNA Mini Kit (Bioline, London, UK) according to the manufacturer's instructions. From mice, the postcaval lobe was homogenized using lysis buffer and quarter-inch ceramic spheres. RNA was next extracted using TRIzol reagent as previously described (17). With the use of SensiFast cDNA Synthesis Kit (Bioline), 0.5  $\mu$ g RNA was reverse transcribed into cDNA. Quantitative real-time PCR was performed by using SYBR Green Master mix (Bioline) on a CFX-96 Real-Time detection system (Bio-Rad CFX-96, Hercules, CA).

Gene expression levels relative to control were calculated using the  $\Delta\Delta$ Ct method normalized to housekeeping genes. Different housekeeping genes were used depending on species and shown in Table 3. For MVECs exposed to shear stress, only one housekeeping gene (ACTB) was used, because of the limited amount of RNA obtained from each experiment. The sequences of primers used are listed in Table 3.

### Western Blot Analysis

Total protein was extracted from human lung MVECs using RIPA buffer supplemented with protease and phosphatase inhibitor cocktail (Thermo Scientific 78443). To obtain sufficient protein for Western blots, one sample consisted of protein isolated from three Ibidi chambers with MVECs exposed to shear stress, whereas for experiments solely consisting of statically cultured MVECs, one sample consisted of MVECs obtained from one well of a six-well plate. Protein lysates were loaded in precast protein gels (4–20% gradient gel, Bio-Rad) and transferred to a PVDF membrane (Amersham Hybond P 0.2 PVDF, GE health, Little Chalfont, UK). After blocking with 5% bovine serum albumin (BSA) (Sigma Aldrich, Houten, The Netherlands) at room temperature for 1 h, the membranes were incubated overnight at 4°C with the primary antibodies listed in Table 4. The membranes were washed with Tris-buffered saline-Tween 20 (TBST) three times for 5 min each, after which they were incubated with horseradish peroxidase-conjugated or fluorescently labeled secondary antibodies at room temperature for 1 h.

Proteins were detected by chemiluminescence using enhanced chemiluminescence substrate (GE Health) or using the Odyssey system (LI-COR Biosciences, Lincoln, NE) according to the manufacturer's protocol. Quantification of bands by densitometry analysis was conducted in Image Studio software (LI-COR Biosciences).

### Immunofluorescence

Cells were grown to confluence in a 12-well plate on a glass coverslip or in ibidi  $\mu$ -Slides. The confluent cell layers were fixed with 4% paraformaldehyde in PBS for 15 min at room temperature, after which cells were washed three times with PBS. The fixed cells were permeabilized with 0.1% Triton X-100 (Sigma Aldrich) for 10 min and blocked with 2% BSA in PBS for 1 h. Thereafter, the samples were put at 4°C overnight with indicated primary antibody

**Table 3. Primer sequences used for quantitative PCR**

Gene	Sense Primer Sequence	Antisense Primer Sequence
Human		
<i>Piezo1</i>	TCGCTGGTCTACCTGCTCTT	GGCCTGTGTGACCTTGGGA
<i>Piezo2</i>	GCCCAACAAAGCCAGTTGAA	GGGCTGATGGTCCACAAAGA
<i>PECAM1</i>	GTGAGGGTCAACTGTTCTGT	GTGACCAGTTCACTCTTGGT
<i>Calponin</i>	TGAAGTACGCAGAGAAGCAG	CAGCTTGGGGTCTGTAGAG
<i>ACTA2</i>	CTATGAGGGCTATGCCTTGCC	GCTCAGCCAGTAGTAACGAAGGA
<i>SM22A</i>	ATCTGGGGCGCTACA	CCAACAAGGGTCCATCCTACG
<i>VE-cadherin</i>	TGACGTGAACGACAACCTGGC	GACGCATTGAACAACCGATG
<i>DSCR1</i>	GAGGACGCATTCCAAATCAT	AGTCCCAAATGTCCCTTGTGC
<i>ACTB</i>	TCCCTGGAGAAGAGCTACGA	AGCACTGTGTGGCGTACAG
<i>GAPDH</i>	TGCCAAATATGATGACATCAAGAA	GGAGTGGGTGTCGCTGTTG
Swine		
<i>Piezo1</i>	GGTCTCTACTGGCTGCTG	CCAGTGTGACCTTGGATGCT
<i>Piezo2</i>	GAGCTGGTGGTCTTCAACGA	ATCCCATAAATGCCGTAGCCG
<i>ACTB</i>	TCCCTGGAGAAGAGCTACGA	AGCACCGTGTGGCGTAGAG
<i>GAPDH</i>	GCTCATTTCTCGTACGACAAT	GAGGGCTCTCCTCCTCGC
<i>Cyclo</i>	AGACAGCAGAAAACCTCCGTG	AAGATGCCAGGACCCGTATG
Mice		
<i>Piezo1</i>	GCTTTTGGGAAGCACTCTGC	AGTTGCCCAAGATACGGGTG
<i>Piezo2</i>	CCAAGTAGCCCATGCAAAT	GCATAACCCTGTGCCAGATT
<i>ACTB</i>	ACTGTGAGTTCGCGTCCA	ATCCATGGCGAACTGGTGG
<i>RPLP0</i>	TTTGACAACGGCAGCATTTA	CCGATCTGCAGACACACACT
Rat		
<i>Piezo1</i>	GACGCCTCACAAGGAAAGC	GGGCAGCATCTATGTATCC
<i>Piezo2</i>	GACAGTATCTCCAGCGAGCC	ATCTGGAGTGAGGCTGACCT

(Table 4). Subsequently, cells were washed three times with PBS, followed by incubation with a fluorescently labeled secondary antibody in 1% BSA, protected from light at room temperature for 1 h. The stained cells were washed three times with PBS and fixed with mounting medium containing DAPI (Vector Lab H1200, Bleiswijk, The Netherlands). Imaging was performed with the Leica SP5 confocal microscope. The images were captured with  $\times 40$  or  $\times 63$  objective. To measure cellular morphology in

different shear stress settings, cells were stained with vascular endothelial (VE)-cadherin to label the cell membranes. Cell alignment to flow was subsequently determined as the length-to-width ratio of individual MVECs by using ImageJ.

### Statistical Analysis

The exact statistical test and number of samples per experiment is specified in the text. Statistical analyses were

**Table 4. Antibodies used in the WB and IF**

Antibodies	Host	Company	Dilution	Used
Primary antibody				
Anti-eNOS/NOS type III	Mouse	BD Biosciences 6190297	1:1,000	WB
Phospho-eNOS (Ser1177) antibody	Rabbit	Cell Signaling 9571S	1:1,000	WB
Akt antibody	Rabbit	Cell Signaling 9272	1:1,000	WB
Phospho-Akt (Ser473)	Rabbit	Cell Signaling 4060	1:2,000	WB
CD31 (PECAM-1) (89C2)	Mouse	Cell Signaling 3528	1:1,000/1:100	WB/IF
GAPDH (14C10)	Rabbit	Cell Signaling 2118	1:1,000	WB
ACTB antibody	Rabbit	Cell Signaling 4967	1:1,000	WB
$\alpha$ -Smooth muscle actin (D4K9N)	Rabbit	Cell Signaling 19245	1:1,000	WB
Anti-TAGLN/transgelin antibody	Rabbit	Abcam ab14106	1:1,000/1:100	WB/IF
Calponin 1 (D8L2T)	Rabbit	Cell Signaling 17819	1:100	IF
VE-cadherin antibody	Mouse	R&D Systems MAB9381	1:100	IF
Secondary antibody				
Anti-rabbit HRP linked		Cell Signaling 7074	1:2,000	WB
Anti-mouse HRP linked		Cell Signaling 7076	1:2,000	WB
IRDye 680RD goat anti-mouse IgG		LI-COR D1014-03	1:5,000	WB
IRDye 680RD goat anti-rabbit IgG		LI-COR D00115-06	1:5,000	WB
Anti-rabbit IgG (H + L) (Alexa Fluor 488 conjugate)		Cell Signaling 4412	1:500	IF
Donkey anti-mouse IgG (H&L) (Alexa Fluor 488)		Abcam ab150105	1:500	IF
Goat anti-mouse IgG (H + L) (Alexa Fluor 568)		Invitrogen A-11004	1:500	IF
Acti-Stain 555 phalloidin		Cytoskeleton PHD1-A	1:100	Actin IF

WB, Western blotting; IF, immunofluorescence; eNOS, endothelial nitric oxide synthase; VE, vascular endothelium; HRP, horseradish peroxidase; H + L, heavy and light chains of the IgG molecule; PECAM, platelet endothelial cell adhesion molecule-1.

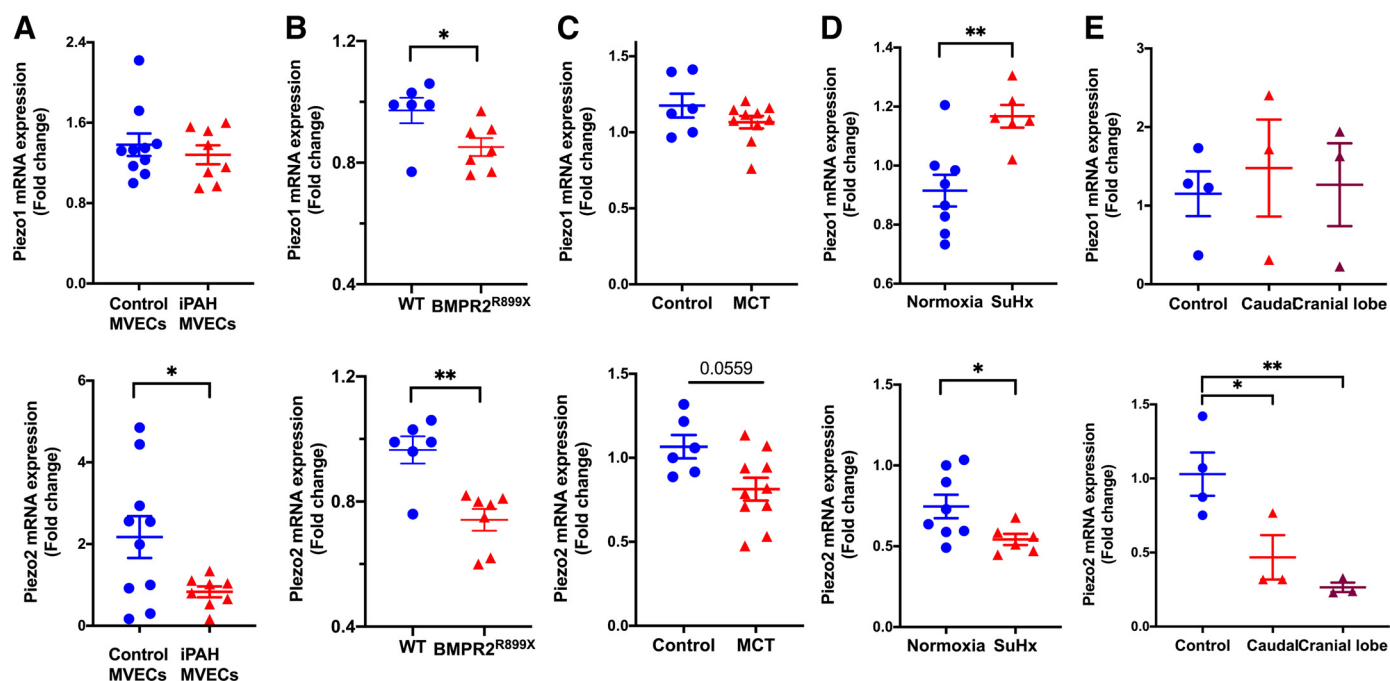


**Figure 1.** Piezo gene expression in lung tissue/MVECs in patients with PAH and PH animal models. *A:* *Piezo1* and *Piezo2* gene expression was quantified by RT-qPCR in pulmonary microvascular endothelial cells (MVECs) isolated from control donors and patients with idiopathic pulmonary arterial hypertension (iPAH). Gene expression was normalized to 18S (control,  $n = 10$ ; and iPAH  $n = 8$ ; unpaired  $t$  test). *B:* *Piezo1* and *Piezo2* gene expression was quantified by RT-qPCR in *Bmpr2*<sup>+/R899X</sup> mice and wild-type (WT) controls. Gene expression was normalized with RPLP0 and ACTB (WT,  $n = 6$ ; and *Bmpr2*<sup>+/R899X</sup> mice,  $n = 7$ ; unpaired  $t$  test). *C:* *Piezo1* and *Piezo2* gene expression was quantified by RT-qPCR in control rats and MCT-PAH rats. Gene expression was normalized to 18S (control,  $n = 6$ ; and MCT rats,  $n = 10$ , unpaired  $t$  test). *D:* *Piezo1* and *Piezo2* gene expression was quantified by RT-qPCR in control normoxia rats and SuHx rats. Gene expression was normalized to 18S (normoxia rats,  $n = 8$ ; and SuHx rats,  $n = 6$ ; unpaired  $t$  test). *E:* *Piezo1* and *Piezo2* gene expression in lung MVECs isolated from control swine and caudal and cranial lobes from PVB swine. Gene expression was normalized with ACTB and GAPDH and Cyclo (control,  $n = 4$ ; PVB caudal lobes,  $n = 3$ ; and PVB cranial lobes,  $n = 3$ ; one-way ANOVA with Tukey's multiple comparison test). \* $P < 0.05$ ; \*\* $P < 0.01$ . MCT, monocrotaline; MVEC, microvascular endothelial cell; PAH, pulmonary arterial hypertension; PH, pulmonary hypertension; SuHx, sugen-hypoxia-induced PH.

performed using GraphPad Prism 9, and  $P < 0.05$  was considered significant. Data are presented as means  $\pm$  SE.

## RESULTS

### Reduced *Piezo2* Gene Expression in PAH: Role of TGF $\beta$ Signaling

Piezo transcription was assessed by RT-qPCR in lung MVECs of patients with PAH, control subjects, as well as in lung tissue of four different animal models of PH (Fig. 1A). Expression of *Piezo2*, but not *Piezo1*, was lower in lung

MVECs of patients with PAH as compared with control subjects. *Bmpr2*<sup>+/R899X</sup> mice, mice with a knock-in of a *BMPR2* mutation commonly found in humans with PAH, showed a reduced expression of both *Piezo1* and *Piezo2* in the lungs (Fig. 1B) at a time point (6 to 7 mo of age) at which right ventricular hypertrophy was present (Table 5) and lesions were found in the pulmonary vasculature (16, 17). Similarly, *Piezo2* expression tended to be reduced in lungs of MCT rats (Fig. 1C,  $P = 0.0559$ ) and was significantly reduced in lungs of SuHx rats (Fig. 1D), whereas *Piezo1* was either increased (SuHx, Fig. 1D) or unaltered (MCT; Fig. 1C). The reduction in *Piezo2* was accompanied by an increase in total pulmonary resistance and right ventricular hypertrophy (Table 6).

**Table 5.** Characteristics of the mouse model

	Controls	<i>Bmpr2</i> <sup>+/R899X</sup> Mice	<i>P</i> Value
<i>n</i>	6	7	
Sex, female/male	4/2	3/4	
Heart rate, beats/min	544 $\pm$ 17	548 $\pm$ 22	0.89
RVSP, mmHg	18.5 $\pm$ 0.5	20.6 $\pm$ 2.3	0.50
Cardiac index, mL/min/g	0.15 $\pm$ 0.02	0.18 $\pm$ 0.02	0.32
Body weight, g	32 $\pm$ 4	30 $\pm$ 3	0.66
RV/BW, mg/g	0.65 $\pm$ 0.07	0.80 $\pm$ 0.04	0.07
LV/BW, mg/g	3.18 $\pm$ 0.22	3.37 $\pm$ 0.21	0.56
Fulton index	0.20 $\pm$ 0.01	0.24 $\pm$ 0.01*	0.026

Values are means  $\pm$  SE; *n*, number of mice. RVSP, right ventricular systolic pressure; RV, right ventricular weight; LV, left ventricular weight; BW, body weight; Fulton index, RV/LV. \* $P < 0.05$  by unpaired  $t$  test.

**Table 6.** Characteristics of the rat models

	Control	SuHx	Control	MCT
Sex, female/male	0/8	0/6	0/6	0/10
Heart rate, beats/min	282 $\pm$ 81	325 $\pm$ 28	334 $\pm$ 28	316 $\pm$ 10
RVSP, mmHg	15 $\pm$ 1	45 $\pm$ 11*	18 $\pm$ 2	45 $\pm$ 4*
Cardiac output, mL/min	97 $\pm$ 9	41 $\pm$ 2*	110 $\pm$ 5	63 $\pm$ 8*
TPR, mmHg/mL/min	160 $\pm$ 22	1,081 $\pm$ 286*	162 $\pm$ 17	735 $\pm$ 123*
Body weight, g	508 $\pm$ 57	456 $\pm$ 64	475 $\pm$ 44	432 $\pm$ 42
Fulton index	0.29 $\pm$ 0.02	0.71 $\pm$ 0.1*	0.32 $\pm$ 0.02	0.75 $\pm$ 0.12

Values are means  $\pm$  SE; *n*, number of rats. SuHx, sugen-hypoxia-induced pulmonary hypertension; MCT, monocrotaline; RVSP, right ventricular systolic pressure; TPR, total pulmonary resistance. \* $P < 0.05$  by unpaired  $t$  test vs. corresponding control group.

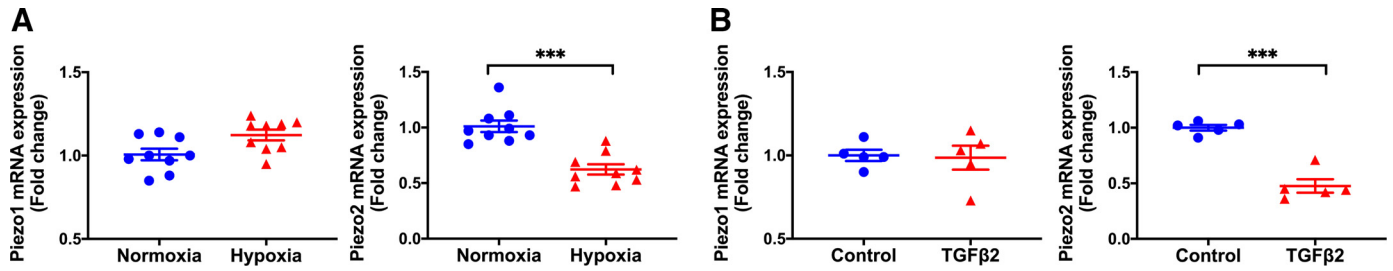


**Figure 2.** Piezo gene expression changes in stimulated human lung MVECs. *A:* *Piezo1* and *Piezo2* gene expression in statically cultured lung microvascular endothelial cells (MVECs) exposed to 21% O<sub>2</sub> (normoxia) or 1% O<sub>2</sub> (hypoxia) for 24 h (*n* = 9, unpaired *t* test). *B:* *Piezo1* and *Piezo2* gene expression in lung MVECs exposed to 10 ng/mL TGFβ<sub>2</sub> for 96 h (*n* = 5, unpaired *t* test). *A* and *B:* gene expression was normalized with ACTB. \*\*\**P* < 0.001. MVEC, microvascular endothelial cell.

To further assess whether disturbed TGFβ signaling and/or hypoxia, well-documented factors involved in the etiology of pulmonary hypertension (25–27), could be causally related to dysregulated Piezo expression, cultured human lung MVECs from healthy donors were treated with TGFβ<sub>2</sub> or exposed to hypoxia. Exposure to TGFβ<sub>2</sub>, as well as to hypoxia, led to a significant reduction in endothelial Piezo2 expression whereas Piezo1 expression was not affected (Fig. 2, *A* and *B*).

### Shear Stress and Piezo Expression

To investigate to what extent exposure to abnormal shear stress in vivo was involved in the altered expression of Piezo2, Piezo expression was evaluated in lung tissue of swine, 12 wk after banding of the confluent of the pulmonary veins draining the caudal lung lobes. As previously described, this banding results in overt pulmonary hypertension (Table 7), with a redistribution of cardiac output from the caudal lung lobes to the cranial lobes, resulting in a mixed phenotype with high pressure/low shear stress in the vasculature draining into the stenotic pulmonary veins (caudal lobes), and high pressure/high shear stress in the vasculature draining into the unaffected pulmonary veins (cranial lobes) (20, 21). Piezo1 mRNA expression was unaltered in both high and low shear stress territories as compared with control swine (Table 7). Conversely, Piezo2 expression was

downregulated in the caudal lobes (low shear stress territories) in comparison with control lung tissue and unaltered in the cranial lobes (high shear stress territories) lung tissue compared with control lung tissue (Table 7). In a subset of animals, MVECs were isolated from lung tissue of the cranial and caudal lobes. Similar to our findings in human MVECs of patients with PAH, in MVECs isolated from both cranial and caudal lobes, Piezo1 expression was unaltered as compared with control, whereas Piezo2 mRNA expression was significantly lower in MVECs isolated from both caudal lobes and cranial lobes as compared with control MVECs (Fig. 1*E*).

To assess a causal relation between the alterations in shear stress and altered Piezo expression, human lung MVECs from healthy donors and patients with PAH were exposed to normal shear stress (21 dyn/cm<sup>2</sup>) and compared with statically cultured MVECs as well as MVECs exposed to high shear stress (67 dyn/cm<sup>2</sup>) (Fig. 3*A*). In MVECs from healthy donors, Piezo1 expression was lower in statically cultured MVECs as compared with MVECs exposed to both normal shear stress and high shear stress, but no difference was found between normal and high shear stress (Fig. 3*B*). However, in line with the findings in swine MVECs, Piezo2 expression was reduced in statically cultured cells and in response to abnormally high shear stress as compared with normal shear stress (Fig. 3*B*). The changes in Piezo2 expression in response to alterations in shear stress were paralleled by changes in the expression of the endothelial markers

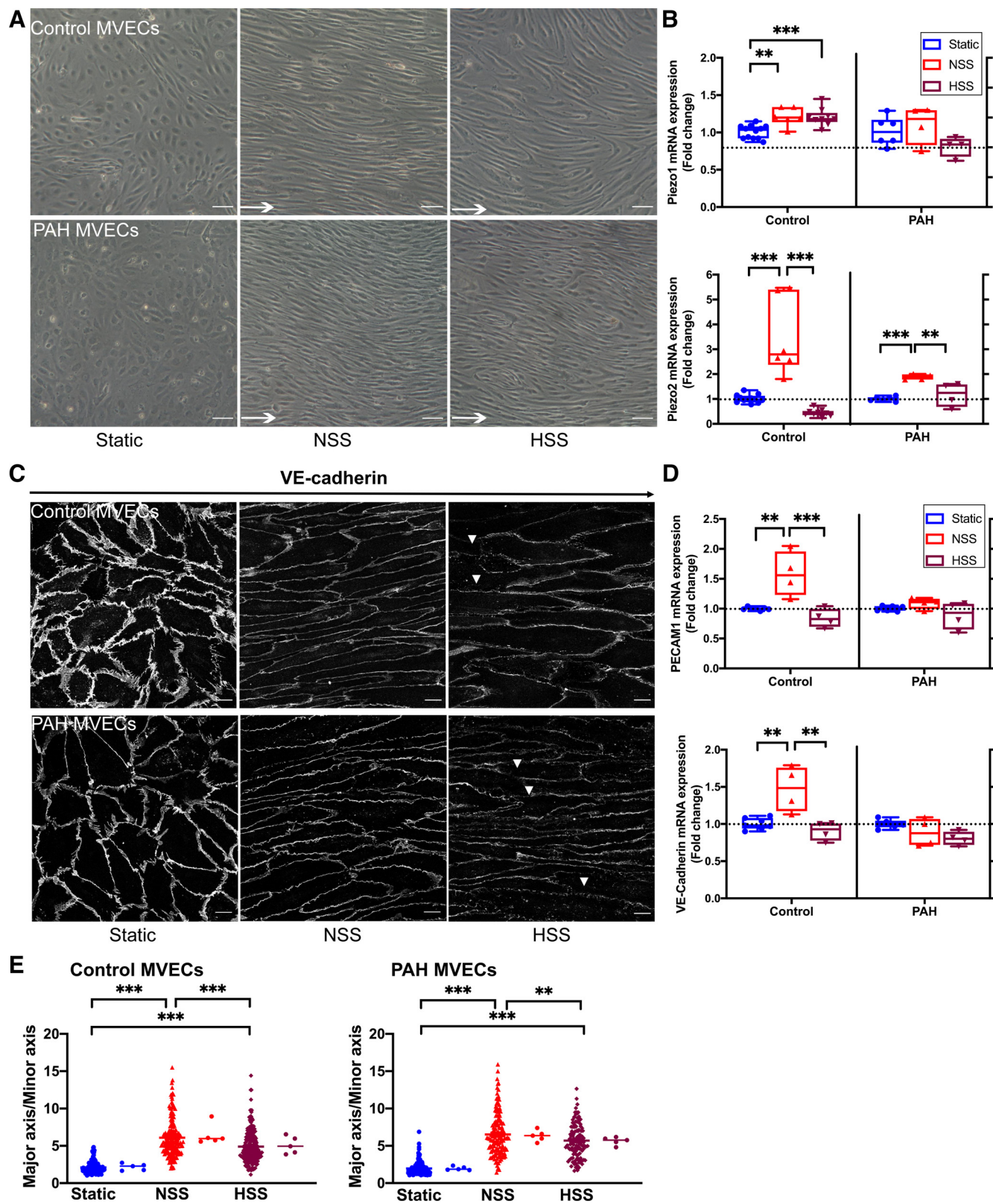
**Table 7.** Characteristics of the swine model

	Control Swine	PVB Swine	<i>P</i> Value
<i>n</i>	8	10	
Sex, female/male	4/4	5/5	
Heart rate, beats/min	132 ± 6	132 ± 4	0.96
Systemic blood pressure, mmHg	88 ± 4	90 ± 4	0.78
Pulmonary artery pressure, mmHg	18.8 ± 1.2	42.9 ± 3.0*	0.000001
Cardiac index, L/min/kg	0.17 ± 0.01	0.17 ± 0.01	0.97
Body weight, kg	59 ± 4	54 ± 4	0.48
RV/BW, g/kg	1.13 ± 0.17	1.73 ± 0.10*	0.006
LV/BW, g/kg	2.64 ± 0.38	3.06 ± 0.11	0.26
Fulton index	0.43 ± 0.01	0.56 ± 0.03*	0.001
Normalized gene expression ( <i>n</i> = 6–9)			
<i>Piezo1</i> (caudal lobes)	1.05 ± 0.06	0.92 ± 0.07	0.64
<i>Piezo2</i> (caudal lobes)	1.25 ± 0.07	0.84 ± 0.12*	0.01
<i>Piezo1</i> (cranial lobes)	0.87 ± 0.05	0.80 ± 0.04	0.32
<i>Piezo2</i> (cranial lobes)	1.02 ± 0.06	1.07 ± 0.14	0.75

Values are means ± SE; *n*, number of swine. PVB, pulmonary vein banding; RV, right ventricular weight; LV, left ventricular weight; BW, body weight; Fulton index, RV/LV. \**P* < 0.05 by unpaired *t* test.

platelet endothelial cell adhesion molecule-1 (PECAM1) and VE-cadherin (Fig. 3D). Interestingly, although Piezo1 expression was unaltered in MVECs from patients with PAH, its altered expression in response to changes in shear stress was

lost. Similarly, expression of PECAM1 and VE cadherin was not influenced by alterations in shear stress in these cells (Fig. 3D). Conversely, although expression of Piezo2 was reduced in MVECs from patients with PAH, modulation of



its expression in response to shear stress was maintained, albeit that difference appeared to be smaller (Fig. 3B). Also, alignment of the MVECs in the direction of flow was maintained in PAH MVECs. Thus, static MVECs exhibited a cobblestone morphology, whereas 72-h exposure to normal shear stress (21 dyn/cm<sup>2</sup>) results in elongated and aligned cells (Fig. 3, A and D), as evidenced by an increase in the length:width ratio (Fig. 3E). In MVECs from both healthy donors and patients with PAH. The length:width ratio was also increased in MVECs exposed to abnormally high shear stress (67 dyn/cm<sup>2</sup>), although some cells appeared to elongate to a spindle shape, suggesting a defective shear response in both groups (Fig. 3, A and C).

These findings, in combination with the transcriptional data from the experimental P(A)H models, provide evidence that various signaling routes, including hypoxia, TGF $\beta$ , and shear stress, may contribute to the altered expression of Piezo2 in PAH, and that alterations in Piezo2 parallel changes in endothelial phenotype in PAH. Given the putative mechanosensory capacities of Piezo channels, we set out to unravel how impaired Piezo2 expression affects endothelial function and vascular remodeling and to what extent this could contribute to progression of microvascular disease in PAH.

### Piezo2 Expression is Essential for Shear-Induced Synthesis of Nitric Oxide

The functional role of Piezo2 as a mechanosensory ion channel was assessed using Piezo2 knockdown in human lung MVECs by siRNA, after which the shear-induced calcium influx in these cells was compared with that in nontargeting siRNA-treated (NT siRNA) control MVECs using the membrane-permeable calcium indicator Fluo-4AM. Piezo2 siRNA strongly reduced Piezo2 mRNA levels in shear-exposed lung MVECs (Fig. 4A), but did not affect Piezo1 expression. Piezo2 siRNA markedly inhibited the shear-induced calcium influx, as evidenced by a lower amplitude of Fluo-4AM intensity compared with MVECs transfected with NT siRNA (Fig. 4B and Supplemental videos S1 and S2; see <https://doi.org/10.6084/m9.figshare.21173878>). Similarly, the peak calcium influx intensity in Piezo2 siRNA-treated cells was significantly lower compared with the NT siRNA-treated MVECs (Fig. 4C). In line with these findings, Down syndrome critical region gene 1 (DSCR1), a small signaling molecule transcriptionally regulated by the Ca<sup>2+</sup>/calmodulin-dependent serine/threonine protein (28), was decreased in MVECs treated with Piezo2 siRNA after 48 h exposure to normal shear stress (Fig. 4D).

To further dissect the consequences of impaired microvascular Piezo2 expression in pulmonary hypertension, endothelial function in the absence of Piezo2 was studied. Shear stress-stimulated nitric oxide (NO) production is dependent on phosphorylation of endothelial NO synthase (eNOS) at Ser1177, which in turn relies on calcium-dependent phosphorylation of AKT (Ser473) (29). Piezo2 knockdown reduced both AKT and eNOS phosphorylation in lung MVECs exposed to 48 h of normal shear stress (Fig. 4, E and F). In line with this reduced activation of eNOS, nitrite + nitrate production in the MVECs' supernatants after shear stress was lower in the supernatants of Piezo2 knockdown MVECs, whereas there was no difference in nitrite + nitrate production in supernatant of static MVECs (Fig. 4G), indicating a lower production of NO in response to shear stress in the absence of Piezo2. Altogether, our results imply that Piezo2 functions as a shear stress-sensitive calcium channel in lung MVECs that participates in shear-dependent NO synthesis.

### Piezo2 is Involved in Shear-Induced Alignment of Endothelial Cells

Normal shear stress plays a key role in maintaining normal vascular structure, whereas abnormally low or high shear stress is a risk factor associated with (pathological) vascular remodeling. Piezo2 siRNA impaired the alignment in response to normal shear stress, with a decrease in length:width ratio as compared with cells treated with nontargeting siRNA (Fig. 5, A and B). Furthermore, staining of filamentous actin (F-actin) suggested a more randomly distributed structure of the cytoskeleton in the Piezo2 siRNA-treated MVECs, all suggesting that Piezo2 is indispensable for a proper adaptation of lung endothelial cells to shear stress (Fig. 5A).

### Impaired Piezo2 Expression Triggers EndMT

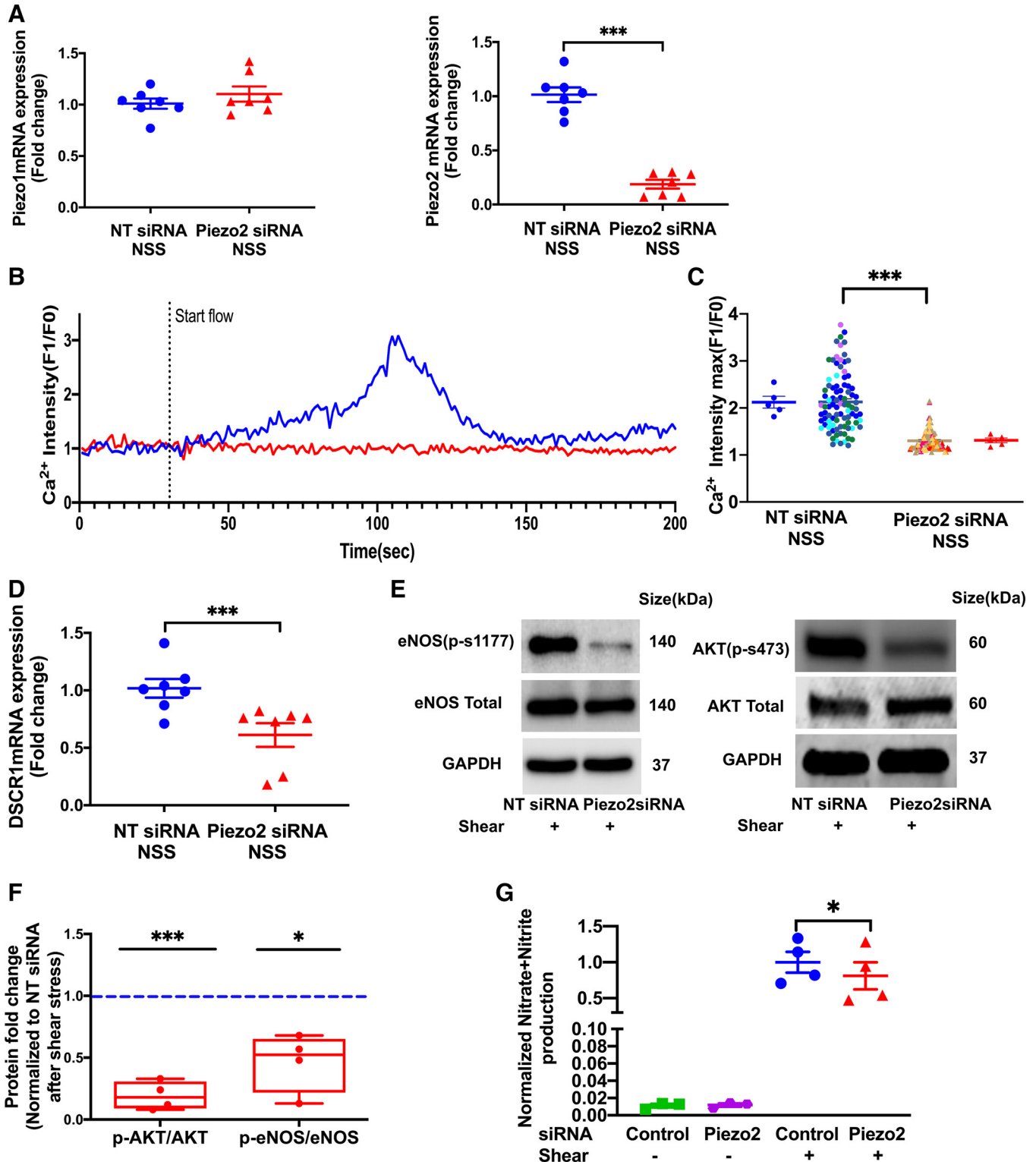
To evaluate the impact of impaired Piezo2 expression on EndMT, a process that could significantly contribute to vascular remodeling and elevated pulmonary resistance (30), lung MVECs were treated with Piezo2 siRNA after which the expression of the endothelial markers PECAM1 and VE-cadherin, as well as the vascular smooth muscle cell (VSMC) markers  $\alpha$ -smooth muscle actin (ACTA2), smooth muscle protein 22- $\alpha$  (SM22A), and Calponin was analyzed. Piezo2 siRNA treatment resulted in a decreased mRNA expression of PECAM1 when compared with nontargeting siRNA-treated MVECs, whereas VE-cadherin levels remained stable. mRNA expression of VSMC markers ACTA2, SM22A, and calponin was significantly increased following Piezo2 siRNA (Fig. 6A). These results were confirmed by immunoblots,

**Figure 3.** Morphological adaptation to shear stress, endothelial markers, and Piezo expression. *A:* representative brightfield microscopy  $\times 10$  magnification images of statically cultured control MVECs and PAH MVECs, and MVECs exposed to normal shear stress (NSS, 21 dyn/cm<sup>2</sup>) or high shear stress (HSS, 67 dyn/cm<sup>2</sup>). Arrows, direction of flow. *B:* *Piezo1* and *Piezo2* gene expression were quantified by RT-qPCR in control MVECs and PAH MVECs that were exposed to NSS (21 dyn/cm<sup>2</sup>) or HSS (67 dyn/cm<sup>2</sup>) or cultured statically. Box plots represent minimum, maximum, median. Fold changes compared with static conditions. Gene expression was normalized to ACTB (control,  $n = 6-12$ ; and PAH,  $n = 4-6$ ; one-way ANOVA with Tukey's multiple comparison test). *C:* representative VE-cadherin (white) immunostaining of control MVECs and PAH MVECs, either statically cultured or after exposure to NSS and HSS. Arrows, direction of flow; arrowheads, areas with low VE-cadherin staining. Scale bar = 20  $\mu$ m. *D:* PECAM1 and VE-cadherin gene expression were quantified by qPCR in control MVECs and PAH MVECs that were exposed to NSS (21 dyn/cm<sup>2</sup>) or HSS (67 dyn/cm<sup>2</sup>) or statically cultured. Box plots represent minimum, maximum, median. Fold changes compared with static conditions. Gene expression was normalized from ACTB (control,  $n = 4-7$ ; and PH,  $n = 4-6$ ; one-way ANOVA with Tukey's multiple comparison test). *E:* quantification of shear adaptation (length-to-width ratio) in different shear stress settings ( $n = 139-209$  single cells, 5 independent experiments; PAH MVECs,  $n = 114-158$  single cells, 5 independent experiments; repeated-measures ANOVA).  $^{**}P < 0.01$ ,  $^{***}P < 0.001$ . MVEC, microvascular endothelial cell; PAH, pulmonary arterial hypertension; PECAM1, platelet endothelial cell adhesion molecule-1.

demonstrating increased protein levels of ACTA2, SM22A and decreased expression of PECAM1 (Fig. 6, D and E). Immunofluorescence images also showed decreased expression of PECAM1 and increased levels of calponin and SM22A in the Piezo2 knockdown MVECs (Fig. 6, B and C). Altogether these results imply that decreased Piezo2

expression may stimulate the transition of lung MVECs toward a more smooth muscle-like phenotype, thereby contributing to vascular remodeling.

Hence, various signaling routes known to be involved in the development of PAH contribute to impaired expression of Piezo2 in pulmonary hypertension, which in turn may



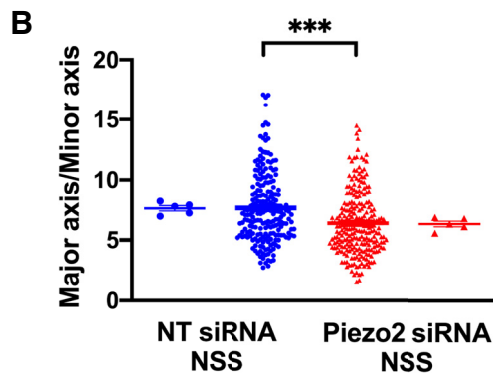
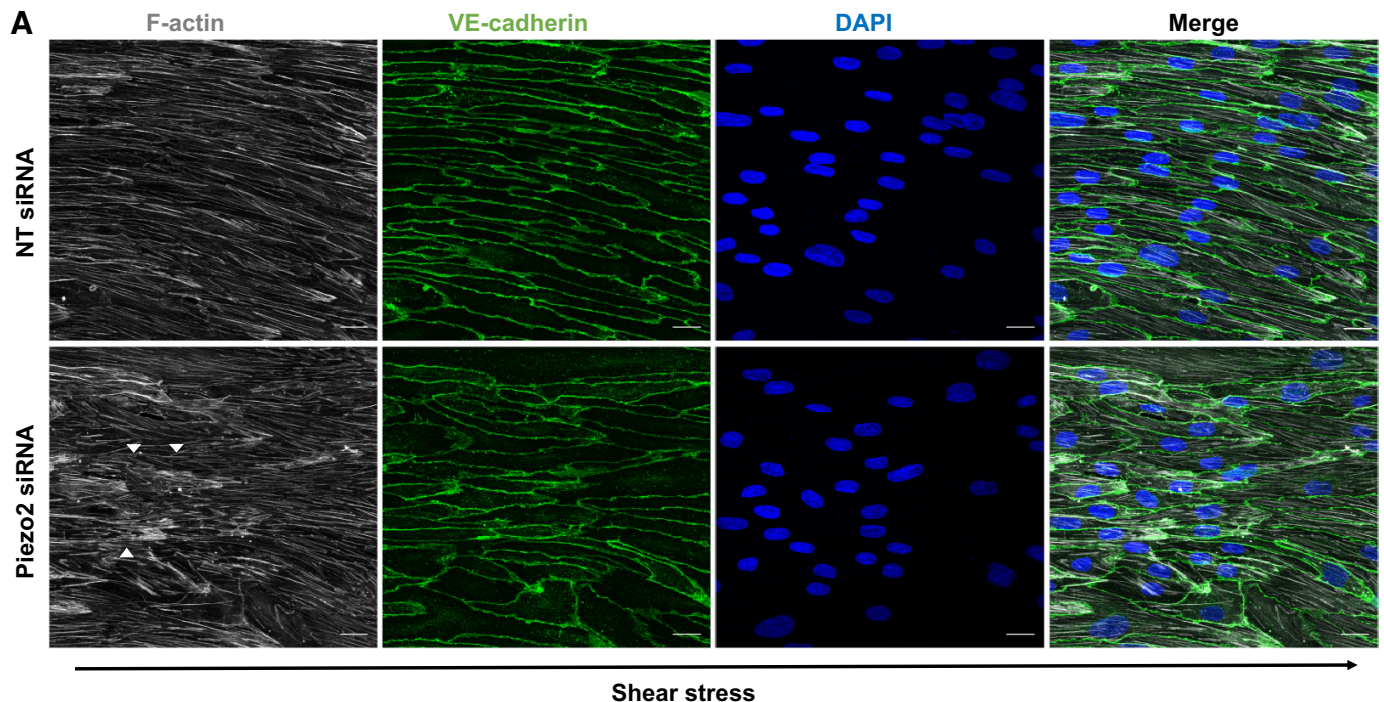


**Figure 5.** *Piezo2* siRNA impairs alignment to normal shear stress. *A*: representative F-actin (white) and VE-cadherin (green) immunostainings of nontargeting (NT) and *Piezo2* siRNA-treated MVECs exposed to NSS. Blue, counterstaining with DAPI; arrow, direction of flow; arrowheads, abnormal F-actin orientation. Scale bar = 20  $\mu\text{m}$ . *B*: quantification of shear adaptation (length-to-width ratio) in NT and *Piezo2* siRNA-treated MVECs after exposure to NSS ( $n = 211$ –246 single cells, 5 independent experiments; repeated-measures ANOVA). \*\*\* $P < 0.001$ . MVEC, microvascular endothelial cell; NSS, normal shear stress.

further the deterioration of vascular tone regulation and induce structural changes in the pulmonary vasculature.

## DISCUSSION

The main findings of our study are summarized in the Fig. 7, and indicate that 1) lung (microvascular endothelial cells) *Piezo2* expression was decreased in human PAH and four different

animal models of P(A)H, and 2) that a dysbalance between TGF $\beta$  and BMP-signaling reduces *Piezo2* expression. 3) *Piezo2* acts as a mechanosensor in lung MVECs regulating intracellular calcium and subsequent NO production in response to shear stress. 4) *Piezo2* is required for endothelial alignment upon exposure to shear stress and that 5) impaired *Piezo2* expression promotes EndMT. The implications of these findings, as well as the limitations of our study will be discussed below.

**Figure 4.** *Piezo2* in acute shear stress-induced responses in human lung MVECs. *A*: *Piezo1* and *Piezo2* gene expression in normal shear stress (21  $\text{dyn}/\text{cm}^2$ )-exposed MVECs after treatment with nontargeting (NT) siRNA or *Piezo2* siRNA ( $n = 7$ , unpaired  $t$  test). *B*: representative single-cell profile of changes in intracellular calcium in MVECs exposed to 21  $\text{dyn}/\text{cm}^2$  shear stress measured by Fluo-4AM. Blue, NT siRNA; red, *Piezo2* siRNA. *C*: quantification the maximal intensity of Fluo-4AM in MVECs exposed to 21  $\text{dyn}/\text{cm}^2$  shear stress [ $n = 81$ –91 single cells, 5 independent experiments (color coded); repeated-measures ANOVA]. *D*: DSCR1 gene expression in shear (21  $\text{dyn}/\text{cm}^2$ )-exposed MVECs after treatment with NT siRNA or *Piezo2* siRNA ( $n = 7$ , unpaired  $t$  test). *E*: representative Western blots of phosphor (p)-eNOS, p-AKT, and GAPDH in shear (21  $\text{dyn}/\text{cm}^2$ )-exposed MVECs after treatment with NT siRNA or *Piezo2* siRNA. *F*: quantification [fold change as compared with NT siRNA (blue) of ratio of p-eNOS to eNOS and the ratio of p-AKT to AKT ( $n = 4$ ; 1 sample  $t$  test with deviation from 1 (=NT siRNA)]. *G*: nitrite + nitrate production in conditioned medium of statically cultured MVECs or after exposure of MVECs to shear stress (21  $\text{dyn}/\text{cm}^2$ ) for 48 h ( $n = 3$  to 4, paired  $t$  test). \* $P < 0.05$ ; \*\*\* $P < 0.001$ . eNOS, endothelial nitric oxide synthase; MVEC, microvascular endothelial cell.



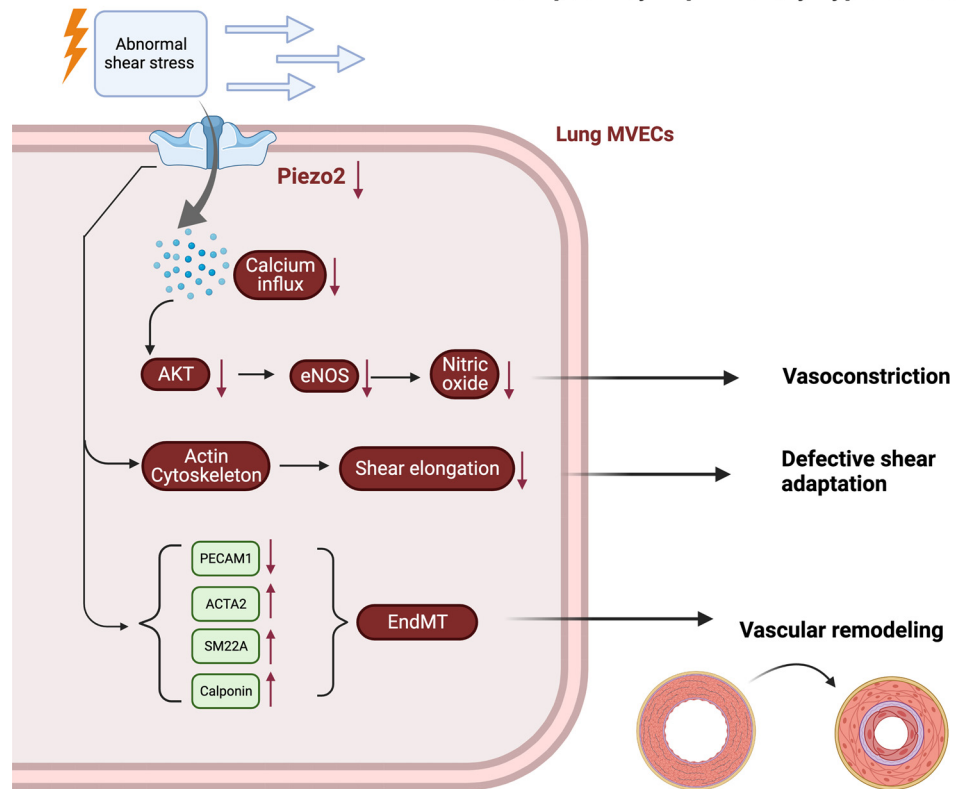


**Figure 7.** Summary of effects of *Piezo2* in the pulmonary microvasculature that may contribute to the development of pulmonary hypertension. Created with Biorender.com, and published with permission.

Alternatively, the difference in Piezo1 expression may reflect alterations in muscularization of the pulmonary microvasculature and/or smooth muscle cell Piezo1 expression, as Piezo1 expression was unaltered in lung MVECs of patients with PAH and swine with PH. Furthermore, the increase in Piezo1 expression in SuHx is consistent with recent findings in lungs of hypoxia exposed rats, although this was most prominent in the endothelial cells (35), which appears to be in contrast with our *in vitro* findings that exposing of MVECs to hypoxia does not alter Piezo1 expression.

Piezo2 is highly expressed in the lung as compared with other organs (36), has been proposed to act as a sensor of lung inflation (37), and previous studies have shown that loss-of-function mutation in the human *PIEZO2* gene causes an autosomal recessive syndrome of muscular atrophy with perinatal respiratory defects (37, 38). Yet, although Piezo2 expression is primarily located to lung endothelial cells (14), a role for Piezo2 in mechanotransduction in the pulmonary circulation had not been studied to date.

Our study shows that Piezo2 expression is reduced in lung MVECs from patients with PAH and swine with type 2 PH secondary to pulmonary vein stenosis as well as in lungs of mice with the *Bmpr2*<sup>+/*R899X*</sup> knock-in mutation and in lungs of rats with MCT- and SuHx-induced PAH. We therefore evaluated stimuli that might alter Piezo2 expression as well as the role of Piezo2 in several processes associated with development and/or progression of P(A)H, including reduced NO production, abnormal endothelial alignment, and EndMT.

### Piezo, Shear Stress, and Endothelial Health

Pulmonary vascular homeostasis requires a healthy endothelium. A key factor in this vascular homeostasis is the endothelial response to shear stress, with production of NO that exerts vasodilator, anti-inflammatory, and antithrombotic effects, thereby contributing to low PVR. Endothelial cells align in the direction of flow and exhibit a quiescent phenotype. Abnormal shear stress levels and abnormal responses to shear stress have been proposed as key factors in the development and progression of pulmonary hypertension. Piezo channels integrate a variety of mechanical stimuli, such as shear stress, tension, and translate them into short-term effects like changes in ion concentrations and long-term effects via changes in gene expression (39).

Actual shear stress levels in the pulmonary microvasculature are currently unknown. Computational modeling estimated that average wall shear stress in the large pulmonary arteries of pediatric patients with PH decreases with increasing disease severity (from 20 to 6 dyn/cm<sup>2</sup>), whereas it increases in the distal small arteries (from 20 to 52 in moderate disease and 116 dyn/cm<sup>2</sup> in severe disease) (3). The data in the human pulmonary vasculature correspond well with data from the healthy porcine pulmonary vasculature at 22 wk of age, with a shear stress of 20 dyn/cm<sup>2</sup> in the main pulmonary artery and around 40–50 dyn/cm<sup>2</sup> in the distal small arteries (40). With a stenosis around the left pulmonary artery, shear stress in the pulmonary small arteries distal to the stenosis decreased to around 18 dyn/cm<sup>2</sup> whereas it increased to around 70 dyn/cm<sup>2</sup> in the unstenosed distal pulmonary vasculature. According to these shear stress computational

measurements, and within the specification of the Ibidi system, normal shear stress values were set at 21 dyn/cm<sup>2</sup> and high shear stress values were at 67 dyn/cm<sup>2</sup>. These shear stress levels are somewhat higher than the “high” shear stress values in previous studies being 14 dyn/cm<sup>2</sup> (5, 41) and 21 dyn/cm<sup>2</sup> (4) respectively, which, based on the studies mentioned (3, 40), do reflect normal shear stress rather than high shear stress as observed in pulmonary hypertension (3).

Mechanosensing and mechanotransduction are required for endothelial responses to shear stress. For this purpose several proteins, including Piezo1, VE-cadherin, and PECAM1 colocalize cell-cell junctions in the cell membrane and form mechanosensing complexes (7). In healthy lung MVECs, Piezo1 transcription increased when these MVECs were exposed to normal and high shear stress, whereas expression of Piezo2 was highest under normal shear stress. Alterations in Piezo1 transcription in response to shear stress were abrogated in MVECs from patients with PAH. Conversely, although Piezo2 expression was reduced in MVECs from patients with PAH, the reduction in expression in response to abnormally high or low shear stress was maintained. Interestingly, in healthy MVECs, alterations in Piezo2 expression were paralleled by changes in VE-cadherin and PECAM1, whereas in MVECs from patients with PAH, the expression pattern of VE-cadherin and PECAM1 resembled Piezo1. Altogether, our findings are consistent with previous observations that the mechanotransduction complex is altered in PAH (4), and for the first time, suggest that Piezo2 is a key component of this complex.

One of the first responses to an increase in shear stress is an elevation in intracellular calcium, subsequent activation of eNOS and production of NO. Mechanosensitive cation channels including transient receptor potential vanilloid 4 (TRPV4) (42, 43) and Piezo1 have been found to play a role in these mechanically induced increases in calcium and NO in pulmonary endothelial cells (13). The present study adds Piezo2 to the list of functional mechanosensitive cation channels in the pulmonary endothelium, by showing that knockdown of the mechanosensitive ion channel Piezo2, which in absence of specific and commercially available antibodies (44, 45) was solely verified on transcriptional level, markedly attenuates the increase in intracellular calcium in response to shear stress, as demonstrated by the strong reduced shear-mediated elevation of Fluo-4AM fluorescence intensity. These findings are in accordance with findings in other cell types, showing that Piezo2 activation leads to a rapid increase in calcium in intestinal epithelium (46) and breast cancer cells (15). Evidence for a more sustained activation of Piezo2 in response to shear stress is provided by our finding that Piezo2 knockdown reduced mRNA expression of DSCR1, a protein that is upregulated in response to increases in intracellular calcium (47), after 48 h of exposure to shear stress.

NO production by eNOS in response to shear stress is enhanced by the calcium/calmodulin induced dissociation from the caveolae followed by eNOS phosphorylation at Ser1177, through the PI3K-AKT pathway (48). Knockdown of Piezo2 reduced both phosphorylation of AKT as well as eNOS at Ser1177 in lung MVECS after 48 h of exposure to shear stress in the present study. These data are consistent with Piezo2-mediated PI3K activation in sensory neurons

mediating touch sensitivity (49, 50) and suggest that activation of AKT is calcium dependent. The latter is consistent with recent studies showing calcium-dependent phosphorylation of AKT using knockdown of Piezo1 (29), although it has previously been proposed that shear stress-induced phosphorylation of AKT is calcium independent (51). Altogether, these findings imply that Piezo2 knockdown reduces intracellular calcium in the presence of shear stress and impairs shear-induced NO production.

In this study, we found that Piezo2, which shows a 42% homology with Piezo1 (8), regulates endothelial NO production in a similar fashion as has previously been shown for Piezo1. Previously, it has been demonstrated that loss of both Piezo1 and Piezo2 in the stretch-sensitive neurons of the baroreceptor complex is required to obliterate the control of heart rate and blood pressure (52), whereas loss of either Piezo1 or Piezo2 impaired the increase in intracellular calcium in response to mechanical stimuli in articular chondrocytes (53). Conversely, data from the present study show no change in Piezo1 following knockdown of Piezo2, and suggest that loss of Piezo2 is sufficient to significantly attenuate phosphorylation of Akt and eNOS and even completely block increase in intracellular calcium. Hence, our results suggest that Piezo2 is a crucial mechanotransduction channel responsible for sensing of and responding to acute changes in shear stress in lung MVECs.

### Role of Piezo2 in Endothelial Alignment in Response to Shear Stress

Prolonged exposure to normal shear stress results in elongation of the endothelial cells in the direction of flow as shown in Fig. 4. Previous studies have shown that endothelial elongation in response to shear stress is perturbed in the lung vasculature of patients with pulmonary hypertension secondary to congenital heart disease in situ (54), and delayed in vitro in lung MVECs isolated from patients with PAH (4). Although Piezo2 expression was lower in MVECs from patients with PAH, Piezo2 was still upregulated, albeit to a lesser extent, in response to normal shear stress, and we found no changes in alignment to shear stress in MVECs from patients with PAH compared with healthy MVECS, although we only evaluated one time point. However, knockdown of Piezo2 with siRNA did impair the alignment to shear stress, which was associated with an altered actin cytoskeletal structure. Similarly, Piezo2 has been shown to control formation of actin-based stress fibers and orientation in breast cancer cells and colocalizes with actin stress fibers in gut epithelial cells (15, 46). Importantly, F-actin reorganization in pulmonary artery endothelial cells was shown to be accompanied by development of mesenchymal morphology (27, 55), which is one of the hallmarks of pulmonary hypertension. Thus, Piezo2 may be a critical factor in pulmonary hypertension, connecting the abnormal shear stress response to endothelial dysfunction including EndMT.

### Role of Piezo2 in Endothelial to Mesenchymal Transition

EndMT involves altered TGF $\beta$  signaling, inflammation, hypoxia as well as altered mechanical forces (25–27). In the present study, we demonstrated that exposure of MVECs to hypoxia or to TGF $\beta$ 2, stimuli known to induce EndMT (56,

57), resulted in a 40–50% reduction in Piezo2 mRNA. Furthermore, a reduced Piezo2 expression, through Piezo2 siRNA, resulted in a reduction in PECAM1 mRNA expression and an increase in ACTA2, SM22A, and calponin. Changes in expression of these markers of EndMT were confirmed at the protein level. A direct link between Piezo2, altered TGF $\beta$  signaling, and EndMT is further suggested by the observation that *Bmpr2*<sup>+ /R899X</sup> mice show a reduced Piezo2 expression in the lungs, at a time that these mice did not show overt pulmonary hypertension, but did show enhanced muscularization of the lung vasculature (16, 17). Similarly, rats with MCT and SuHx-induced PAH, that show increased circulating TGF $\beta$  levels, higher TGF $\beta$ -R2 levels in, and increased muscularization of the pulmonary vasculature, showed reduced Piezo2 levels in the lung. Although a direct link between the increased muscularization and the loss of Piezo2 remains to be established, it is likely that reduced Piezo2, either through impaired NO production in the MVECs, with subsequent reduction in cGMP-mediated inhibition of smooth muscle cell proliferation or through a direct activation of EndMT, plays a central role in this pulmonary vascular remodeling. Taken together, the fact that Piezo2 is reduced in response to stimuli known to induce EndMT and that loss of Piezo2 induces a gene and protein expression pattern consistent with EndMT, suggests that Piezo2 may be a novel player in this process.

### Conclusions and Perspective

Our findings suggest that Piezo2 is an important mechanosensor that is essential to maintain normal pulmonary microvascular endothelial function. Loss of Piezo2 expression in lung microvascular endothelial cells, as observed in patients with PAH and four separate animal models, reflecting different aspects of pulmonary (arterial) hypertension, could facilitate disease progression by limiting both NO production and alignment in response to shear stress, as well as by promoting EndMT (Fig. 7). Till date, Piezo2-specific antibodies, agonists or antagonists are not available, but, to further substantiate the importance and therapeutic potential of targeting Piezo2 in pulmonary hypertension, future studies incorporating these compounds will be essential.

### DATA AVAILABILITY

Uncut Western Blots are available in the online data supplement.

### SUPPLEMENTAL DATA

Supplemental Videos S1 and S2: <https://doi.org/10.6084/m9.figshare.21173878>.

### ACKNOWLEDGMENTS

We are grateful for the help of Prof. Marie José Goumans and Dr. Kondababu Kurakula from Leiden University Medical Center with the Ibidi system. We thank the ErasmusMC Optical Imaging Center for assistance with calcium measurements and analysis.

Present address of Z. Cai: The Second Affiliated Hospital Zhejiang University School of Medicine, Zhejiang, People's Republic of China.

### GRANTS

This work was supported by the China Scholarship Council Grants 201708130077 (to S.T.) and 201606230252 (to Z.C.), China Postdoctoral Science Foundation Grant 2020M680079 (to Z.C.), Dutch Cardiovascular Alliance Grant DCVA-RECONNECT (to D.M. and M.B.), and German Center for Cardiovascular Research Grant DZHK81Z0600207 (to D.M. and P.S.).

### DISCLOSURES

No conflicts of interest, financial or otherwise, are declared by the authors.

### AUTHOR CONTRIBUTIONS

S.T., M.M.B., and D.M. conceived and designed research; S.T., D.v.U., E.v.d.K., and R.T. performed experiments; S.T., D.v.U., R.T., and L.T. analyzed data; S.T., Z.C., P.S., L.T., C.G., K.V.d.H., M.M.B., and D.M. interpreted results of experiments; S.T. prepared figures; S.T., M.M.B., and D.M. drafted manuscript; S.T., Z.C., P.S., D.v.U., E.v.d.K., K.B., K.V.d.H., M.M.B., and D.M., edited and revised manuscript; S.T., Z.C., P.S., D.v.U., E.v.d.K., R.T., L.T., C.G., K.B., K.V.d.H., M.M.B., and D.M. approved final version of manuscript.

### REFERENCES

1. Budhiraja R, Tudor RM, Hassoun PM. Endothelial dysfunction in pulmonary hypertension. *Circulation* 109: 159–165, 2004. doi:10.1161/01.CIR.0000102381.57477.50.
2. Ando J, Yamamoto K. Flow detection and calcium signalling in vascular endothelial cells. *Cardiovasc Res* 99: 260–268, 2013. doi:10.1093/cvr/cvt084.
3. Yang W, Dong M, Rabinovitch M, Chan FP, Marsden AL, Feinstein JA. Evolution of hemodynamic forces in the pulmonary tree with progressively worsening pulmonary arterial hypertension in pediatric patients. *Biomech Model Mechanobiol* 18: 779–796, 2019. doi:10.1007/s10237-018-01114-0.
4. Szulcek R, Happé CM, Rol N, Fontijn RD, Dickhoff C, Hartemink KJ, Grünberg K, Tu L, Timens W, Nossent GD, Paul MA, Leyen TA, Horrevoets AJ, de Man FS, Guignabert C, Yu PB, Vonk-Noordegraaf A, van Nieuw Amerongen GP, Bogaard HJ. Delayed microvascular shear adaptation in pulmonary arterial hypertension. Role of platelet endothelial cell adhesion molecule-1 cleavage. *Am J Respir Crit Care Med* 193: 1410–1420, 2016. doi:10.1164/rccm.201506-1231OC.
5. Li M, Scott DE, Shandas R, Stenmark KR, Tan W. High pulsatility flow induces adhesion molecule and cytokine mRNA expression in distal pulmonary artery endothelial cells. *Ann Biomed Eng* 37: 1082–1092, 2009. doi:10.1007/s10439-009-9684-3.
6. Lu X, Gong J, Dennery PA, Yao H. Endothelial-to-mesenchymal transition: pathogenesis and therapeutic targets for chronic pulmonary and vascular diseases. *Biochem Pharmacol* 168: 100–107, 2019. doi:10.1016/j.bcp.2019.06.021.
7. Tian S, Steenhorst JJ, van der Heiden K, Merkus D. Mechanosensing and mechanotransduction in pulmonary hypertension. In: *Vascular Mechanobiology in Physiology and Disease*, edited by Hecker M, Duncker DJ. Cham: Springer International Publishing, 2021, p. 299–318.
8. Coste B, Mathur J, Schmidt M, Earley TJ, Ranade S, Petrus MJ, Dubin AE, Patapoutian A. Piezo1 and Piezo2 are essential components of distinct mechanically activated cation channels. *Science* 330: 55–60, 2010. doi:10.1126/science.1193270.
9. Ranade SS, Qiu Z, Woo SH, Hur SS, Murthy SE, Cahalan SM, Xu J, Mathur J, Bandell M, Coste B, Li YS, Chien S, Patapoutian A. Piezo1, a mechanically activated ion channel, is required for vascular development in mice. *Proc Natl Acad Sci USA* 111: 10347–10352, 2014. doi:10.1073/pnas.1409233111.
10. Li J, Hou B, Tumova S, Muraki K, Bruns A, Ludlow MJ, Sedo A, Hyman AJ, McKeown L, Young RS, Yuldasheva NY, Majeed Y, Wilson LA, Rode B, Bailey MA, Kim HR, Fu Z, Carter DA, Bilton J,

- Imrie H, Ajuh P, Dear TN, Cubbon RM, Kearney MT, Prasad RK, Evans PC, Ainscough JF, Beech DJ. Piezo1 integration of vascular architecture with physiological force. *Nature* 515: 279–282, 2014. doi:10.1038/nature13701.
11. Albarrán-Juárez J, Iring A, Wang S, Joseph S, Grimm M, Strilic B, Wettschureck N, Althoff TF, Offermanns S. Piezo1 and Gq/G11 promote endothelial inflammation depending on flow pattern and integrin activation. *J Exp Med* 215: 2655–2672, 2018. doi:10.1084/jem.20180483.
  12. Wang S, Chennupati R, Kaur H, Iring A, Wettschureck N, Offermanns S. Endothelial cation channel PIEZO1 controls blood pressure by mediating flow-induced ATP release. *J Clin Invest* 126: 4527–4536, 2016. doi:10.1172/JCI87343.
  13. Lhomme A, Gilbert G, Pele T, Deweirdt J, Henrion D, Baudrimont I, Campagnac M, Marthan R, Guibert C, Ducret T, Savineau JP, Quignard JF. Stretch-activated Piezo1 channel in endothelial cells relaxes mouse intrapulmonary arteries. *Am J Respir Cell Mol Biol* 60: 650–658, 2019. doi:10.1165/rcmb.2018-0197OC.
  14. Hong J, Arneson D, Umar S, Ruffenach G, Cunningham CM, Ahn IS, Diamante G, Bhetraratana M, Park JF, Said E, Huynh C, Le T, Medzikovic L, Humbert M, Soubrier F, Montani D, Girerd B, Tregouët DA, Channick R, Saggar R, Eghbali M, Yang X. Single-cell study of two rat models of pulmonary arterial hypertension reveals connections to human pathobiology and drug repositioning. *Am J Respir Crit Care Med* 203: 1006–1022, 2021. doi:10.1164/rccm.202006-2169OC.
  15. Pardo-Pastor C, Rubio-Moscardo F, Vogel-González M, Serra SA, Afthinos A, Mrkonjic S, Destaing O, Abenza JF, Fernández-Fernández JM, Trepast X, Albiges-Rizo C, Konstantopoulos K, Valverde MA. Piezo2 channel regulates RhoA and actin cytoskeleton to promote cell mechanobiological responses. *Proc Natl Acad Sci USA* 115: 1925–1930, 2018. doi:10.1073/pnas.1718177115.
  16. Long L, Ormiston ML, Yang X, Southwood M, Gräf S, Machado RD, Mueller M, Kinzel B, Yung LM, Wilkinson JM, Moore SD, Drake KM, Aldred MA, Yu PB, Upton PD, Morrell NW. Selective enhancement of endothelial BMPRII with BMP9 reverses pulmonary arterial hypertension. *Nat Med* 21: 777–785, 2015. doi:10.1038/nm.3877.
  17. van Uden D, Koudstaal T, van Hulst JAC, Bergen IM, Gootjes C, Morrell NW, van Loo G, von der Thusen JH, van den Bosch TPP, Ghigna MR, Perros F, Montani D, Kool M, Boomars KA, Hendriks RW. Central role of dendritic cells in pulmonary arterial hypertension in human and mice. *Int J Mol Sci* 22: 1756, 2021. doi:10.3390/ijms22041756.
  18. Cai Z, Tian S, Klein T, Tu L, Geenen LW, Koudstaal T, van den Bosch AE, de Rijke YB, Reiss IKM, Boersma E, van der Ley C, Van Faassen M, Kema I, Duncker DJ, Boomars KA, Tran-Lundmark K, Guignabert C, Merkus D. Kynurenine metabolites predict survival in pulmonary arterial hypertension: a role for IL-6/IL-6R $\alpha$ . *Sci Rep* 12: 12326, 2022. doi:10.1038/s41598-022-15039-3.
  19. Tu L, Desroches-Castan A, Mallet C, Guyon L, Cumont A, Phan C, Robert F, Thuillet R, Bordenave J, Sekine A, Huertas A, Ritvos O, Savale L, Feige JJ, Humbert M, Bailly S, Guignabert C. Selective BMP-9 inhibition partially protects against experimental pulmonary hypertension. *Circ Res* 124: 846–855, 2019. doi:10.1161/CIRCRESAHA.118.313356.
  20. van Duin RWB, Stam K, Uitterdijk A, Bartelds B, Danser AHJ, Reiss IKM, Duncker DJ, Merkus D. Intervening with the nitric oxide pathway to alleviate pulmonary hypertension in pulmonary vein stenosis. *J Clin Med* 8: 1204, 2019. doi:10.3390/jcm8081204.
  21. van Duin RWB, Stam K, Cai Z, Uitterdijk A, Garcia-Alvarez A, Ibanez B, Danser AHJ, Reiss IKM, Duncker DJ, Merkus D. Transition from post-capillary pulmonary hypertension to combined pre- and post-capillary pulmonary hypertension in swine: a key role for endothelin. *J Physiol* 597: 1157–1173, 2019. doi:10.1113/JP275987.
  22. Comhair SA, Xu W, Mavrikis L, Aldred MA, Asosingh K, Erzurum SC. Human primary lung endothelial cells in culture. *Am J Respir Cell Mol Biol* 46: 723–730, 2012. doi:10.1165/rcmb.2011-0416TE.
  23. Tu L, Dewachter L, Gore B, Fadel E, Dartevielle P, Simonneau G, Humbert M, Eddahibi S, Guignabert C. Autocrine fibroblast growth factor-2 signaling contributes to altered endothelial phenotype in pulmonary hypertension. *Am J Respir Cell Mol Biol* 45: 311–322, 2011. doi:10.1165/rcmb.2010-0317OC.
  24. van der Feen DE, Bartelds B, de Boer RA, Berger RMF. Assessment of reversibility in pulmonary arterial hypertension and congenital heart disease. *Heart* 105: 276–282, 2019. doi:10.1136/heartjnl-2018-314025.
  25. Kovacic JC, Dimmeler S, Harvey RP, Finkel T, Aikawa E, Krenning G, Baker AH. Endothelial to mesenchymal transition in cardiovascular disease: JACC state-of-the-art review. *J Am Coll Cardiol* 73: 190–209, 2019. doi:10.1016/j.jacc.2018.09.089.
  26. Stenmark KR, Frid M, Perros F. Endothelial-to-mesenchymal transition: an evolving paradigm and a promising therapeutic target in PAH. *Circulation* 133: 1734–1737, 2016. doi:10.1161/CIRCULATIONAHA.116.022479.
  27. Szulcek R, Sanchez-Duffhues G, Rol N, Pan X, Tsonaka R, Dickhoff C, Yung LM, Manz XD, Kurakula K, Kietbasa SM, Mei H, Timens W, Yu PB, Bogaard H-J, Goumans M-J. Exacerbated inflammatory signaling underlies aberrant response to BMP9 in pulmonary arterial hypertension lung endothelial cells. *Angiogenesis* 23: 699–714, 2020. doi:10.1007/s10456-020-09741-x.
  28. Hesser BA, Liang XH, Camenisch G, Yang S, Lewin DA, Scheller R, Ferrara N, Gerber HP. Down syndrome critical region protein 1 (DSCR1), a novel VEGF target gene that regulates expression of inflammatory markers on activated endothelial cells. *Blood* 104: 149–158, 2004. doi:10.1182/blood-2004-01-0273.
  29. Wang Z, Chen J, Babicheva A, Jain PP, Rodriguez M, Ayon RJ, Ravellette KS, Wu L, Balistrieri F, Tang H, Wu X, Zhao T, Black SM, Desai AA, Garcia JGN, Sun X, Shyy JY, Valdez-Jasso D, Thistlethwaite PA, Makino A, Wang J, Yuan JX. Endothelial upregulation of mechanosensitive channel Piezo1 in pulmonary hypertension. *Am J Physiol Cell Physiol* 321: C1010–C1027, 2021. doi:10.1152/ajpcell.00147.2021.
  30. Reynolds AM, Holmes MD, Danilov SM, Reynolds PN. Targeted gene delivery of BMPRII attenuates pulmonary hypertension. *Eur Respir J* 39: 329–343, 2012. doi:10.1183/09031936.00187310.
  31. Liao J, Lu W, Chen Y, Duan X, Zhang C, Luo X, Lin Z, Chen J, Liu S, Yan H, Chen Y, Feng H, Zhou D, Chen X, Zhang Z, Yang Q, Liu X, Tang H, Li J, Makino A, Yuan JX, Zhong N, Yang K, Wang J. Upregulation of Piezo1 (Piezo type mechanosensitive ion channel component 1) enhances the intracellular free calcium in pulmonary arterial smooth muscle cells from idiopathic pulmonary arterial hypertension patients. *Hypertension* 77: 1974–1989, 2021. doi:10.1161/HYPERTENSIONAHA.120.16629.
  32. Johnson JA, Hemnes AR, Perrien DS, Schuster M, Robinson LJ, Gladson S, Loibner H, Bai S, Blackwell TR, Tada Y, Harral JW, Talati M, Lane KB, Fagan KA, West J. Cytoskeletal defects in Bmpr2-associated pulmonary arterial hypertension. *Am J Physiol Lung Cell Mol Physiol* 302: L474–L484, 2012. doi:10.1152/ajplung.00202.2011.
  33. West J, Harral J, Lane K, Deng Y, Ickes B, Crona D, Albu S, Stewart D, Fagan K. Mice expressing BMPRII transgene in smooth muscle develop pulmonary vascular lesions. *Am J Physiol Lung Cell Mol Physiol* 295: L744–L755, 2008. doi:10.1152/ajplung.90255.2008.
  34. Nourse JL, Pathak MM. How cells channel their stress: interplay between Piezo1 and the cytoskeleton. *Semin Cell Dev Biol* 71: 3–12, 2017. doi:10.1016/j.semcdb.2017.06.018.
  35. Porto Ribeiro T, Barbeau S, Baudrimont I, Vacher P, Freund-Michel V, Cardouat G, Berger P, Guibert C, Ducret T, Quignard JF. Piezo1 channel activation reverses pulmonary artery vasoconstriction in an early rat model of pulmonary hypertension: the role of Ca<sup>2+</sup> influx and Akt-eNOS pathway. *Cells* 11: 2349, 2022. doi:10.3390/cells11152349.
  36. Szczot M, Pogorzala LA, Solinski HJ, Young L, Yee P, Le Pichon CE, Chesler AT, Hoon MA. Cell-type-specific splicing of Piezo2 regulates mechanotransduction. *Cell Rep* 21: 2760–2771, 2017. doi:10.1016/j.celrep.2017.11.035.
  37. Nonomura K, Woo SH, Chang RB, Gillich A, Qiu Z, Francisco AG, Ranade SS, Liberles SD, Patapoutian A. Piezo2 senses airway stretch and mediates lung inflation-induced apnoea. *Nature* 541: 176–181, 2017. doi:10.1038/nature20793.
  38. Delle Vedove A, Storbeck M, Heller R, Hölker I, Hebbar M, Shukla A, Magnusson O, Cirak S, Girisha KM, O'Driscoll M, Loeys B, Wirth B. Biallelic loss of proprioception-related PIEZO2 causes muscular atrophy with perinatal respiratory distress, arthrogryposis, and scoliosis. *Am J Hum Genet* 99: 1206–1216, 2016 [Erratum in *Am J Hum Genet* 99: 1406–1408, 2016]. doi:10.1016/j.ajhg.2016.09.019.

39. **Parpaite T, Coste B.** Piezo channels. *Curr Biol* 27: R250–R252, 2017. doi:10.1016/j.cub.2017.01.048.
40. **Pewowaruk R, Lamers L, Roldán-Alzate A.** Longitudinal evolution of pulmonary artery wall shear stress in a swine model of pulmonary artery stenosis and stent interventions. *Ann Biomed Eng* 49: 1477–1492, 2021. doi:10.1007/s10439-020-02696-6.
41. **Li M, Tan Y, Stenmark KR, Tan W.** High pulsatility flow induces acute endothelial inflammation through overpolarizing cells to activate NF- $\kappa$ B. *Cardiovasc Eng Technol* 4: 26–38, 2013. doi:10.1007/s13239-012-0115-5.
42. **Marziano C, Hong K, Cope EL, Kotlikoff MI, Isakson BE, Sonkusare SK.** Nitric oxide-dependent feedback loop regulates transient receptor potential vanilloid 4 (TRPV4) channel cooperativity and endothelial function in small pulmonary arteries. *J Am Heart Assoc* 6: e007157, 2017. doi:10.1161/JAHA.117.007157.
43. **Daneva Z, Marziano C, Ottolini M, Chen YL, Baker TM, Kuppusamy M, Zhang A, Ta HQ, Reagan CE, Mihalek AD, Kasetti RB, Shen Y, Isakson BE, Minshall RD, Zode GS, Goncharova EA, Laubach VE, Sonkusare SK.** Caveolar peroxynitrite formation impairs endothelial TRPV4 channels and elevates pulmonary arterial pressure in pulmonary hypertension. *Proc Natl Acad Sci USA* 118: e2023130118, 2021. doi:10.1073/pnas.2023130118.
44. **Della Pietra A, Mikhailov N, Giniatullin R.** The emerging role of mechanosensitive piezo channels in migraine pain. *Int J Mol Sci* 21: 696, 2020. doi:10.3390/ijms21030696.
45. **Alper SL.** Genetic diseases of Piezo1 and Piezo2 dysfunction. *Curr Top Membr* 79: 97–134, 2017. doi:10.1016/bs.ctm.2017.01.001.
46. **Alcaino C, Knutson KR, Treichel AJ, Yildiz G, Strega PR, Linden DR, Li JH, Leiter AB, Szurszewski JH, Farrugia G, Beyder A.** A population of gut epithelial enterochromaffin cells is mechanosensitive and requires Piezo2 to convert force into serotonin release. *Proc Natl Acad Sci USA* 115: E7632–E7641, 2018. doi:10.1073/pnas.1804938115.
47. **Brandt MM, van Dijk CGM, Chrifi I, Kool HM, Bürgisser PE, Louzao-Martinez L, Pei J, Rottier RJ, Verhaar MC, Duncker DJ, Cheng C.** Endothelial loss of Fzd5 stimulates PKC/Ets1-mediated transcription of Angpt2 and Flt1. *Angiogenesis* 21: 805–821, 2018. doi:10.1007/s10456-018-9625-6.
48. **Farah C, Michel LYM, Balligand JL.** Nitric oxide signalling in cardiovascular health and disease. *Nat Rev Cardiol* 15: 292–316, 2018. doi:10.1038/nrcardio.2017.224.
49. **Del Rosario JS, Yudin Y, Su S, Hartle CM, Mirshahi T, Rohacs T.** Gi-coupled receptor activation potentiates Piezo2 currents via G $\beta$  $\gamma$ . *EMBO Rep* 21: e49124, 2020. doi:10.15252/embr.201949124.
50. **Narayanan P, Hütte M, Kudryasheva G, Taberner FJ, Lechner SG, Rehfeldt F, Gomez-Varela D, Schmidt M.** Myotubularin related protein-2 and its phospholipid substrate PIP2 control Piezo2-mediated mechanotransduction in peripheral sensory neurons. *eLife* 7: e32346, 2018. doi:10.7554/eLife.32346.
51. **Dimmeler S, Fleming I, Fissithaler B, Hermann C, Busse R, Zeiher AM.** Activation of nitric oxide synthase in endothelial cells by Akt-dependent phosphorylation. *Nature* 399: 601–605, 1999. doi:10.1038/21224.
52. **Zeng WZ, Marshall KL, Min S, Daou I, Chappleau MW, Abboud FM, Liberles SD, Patapoutian A.** PIEZO2s mediate neuronal sensing of blood pressure and the baroreceptor reflex. *Science* 362: 464–467, 2018. doi:10.1126/science.aau6324.
53. **Lee W, Leddy HA, Chen Y, Lee SH, Zelenski NA, McNulty AL, Wu J, Beicker KN, Coles J, Zauscher S, Grandl J, Sachs F, Guilak F, Liedtke WB.** Synergy between Piezo1 and Piezo2 channels confers high-strain mechanosensitivity to articular cartilage. *Proc Natl Acad Sci USA* 111: E5114–E5122, 2014. doi:10.1073/pnas.1414298111.
54. **Rabinovitch M, Bothwell T, Hayakawa BN, Williams WG, Trusler GA, Rowe RD, Olley PM, Cutz E.** Pulmonary artery endothelial abnormalities in patients with congenital heart defects and pulmonary hypertension. A correlation of light with scanning electron microscopy and transmission electron microscopy. *Lab Invest* 55: 632–653, 1986.
55. **Good RB, Gilbane AJ, Trinder SL, Denton CP, Coghlan G, Abraham DJ, Holmes AM.** Endothelial to mesenchymal transition contributes to endothelial dysfunction in pulmonary arterial hypertension. *Am J Pathol* 185: 1850–1858, 2015. doi:10.1016/j.ajpath.2015.03.019.
56. **Ma J, Sanchez-Duffhues G, Goumans MJ, Ten Dijke P.** TGF- $\beta$ -induced endothelial to mesenchymal transition in disease and tissue engineering. *Front Cell Dev Biol* 8: 260, 2020. doi:10.3389/fcell.2020.00260.
57. **Zhang B, Niu W, Dong HY, Liu ML, Luo Y, Li ZC.** Hypoxia induces endothelial-mesenchymal transition in pulmonary vascular remodeling. *Int J Mol Med* 42: 270–278, 2018. doi:10.3892/ijmm.2018.3584.